

## A Reduction in Intestinal Cell pH<sub>i</sub> Due to Loss of the *Caenorhabditis elegans* Na<sup>+</sup>/H<sup>+</sup> Exchanger NHX-2 Increases Life Span\*

Received for publication, July 9, 2003, and in revised form, August 18, 2003  
Published, JBC Papers in Press, August 25, 2003, DOI 10.1074/jbc.M307351200

Keith Nehrke‡

From the Gastroenterology Unit, Department of Medicine, University of Rochester Medical Center, Rochester, New York 14642

Na<sup>+</sup>/H<sup>+</sup> exchangers are involved in cell volume regulation, fluid secretion and absorption, and pH homeostasis. NHX-2 is a *Caenorhabditis elegans* Na<sup>+</sup>/H<sup>+</sup> exchanger expressed exclusively at the apical membrane of intestinal epithelial cells. The inactivation of various intestinal nutrient transport proteins has been shown previously to influence aging via metabolic potential and a mechanism resembling caloric restriction. We report here a functional coupling of NHX-2 activity with nutrient uptake that results in long lived worms. Gene inactivation of *nhx-2* by RNAi led to a loss of fat stores in the intestine and a 40% increase in longevity. The NHX-2 protein was coincidentally expressed with OPT-2, an oligopeptide transporter that is driven by a transmembrane proton gradient and that is also known to be involved in fat accumulation. Gene inactivation of *opt-2* led to a phenotype resembling that of *nhx-2*, although not as severe. In order to explore this potential functional interaction, we combined RNA interference with a genetically encoded, fluorescence-based reagent to measure intestinal intracellular pH (pH<sub>i</sub>) in live worms under physiological conditions. Our results suggest first that OPT-2 is the main dipeptide uptake pathway in the nematode intestine, and second that dipeptide uptake results in intestinal cell acidification, and finally that recovery following dipeptide-induced acidification is normally a function of NHX-2. The loss of NHX-2 protein results in decreased steady-state intestinal cell pH<sub>i</sub>, and we hypothesize that this change perturbs proton-coupled nutrient uptake processes such as performed by OPT-2. Our data demonstrate a functional role for a Na<sup>+</sup>/H<sup>+</sup> exchanger in nutrient absorption *in vivo* and lays the groundwork for examining integrated acid-base physiology in a non-mammalian model organism.

Na<sup>+</sup>/H<sup>+</sup> exchangers mediate the electroneutral transfer of extracellular Na<sup>+</sup> for an intracellular H<sup>+</sup> (for review see Refs. 1–3). To date, eight electroneutral Na<sup>+</sup>/H<sup>+</sup> exchange (NHE)<sup>1</sup> family members have been identified in mammalian organ-

isms, and several isoforms are expressed in the gastrointestinal tract (4). This class of protein has been implicated in cell volume regulation, net bicarbonate movement, and Na<sup>+</sup> reabsorption and is thought to have a housekeeping role in maintaining pH homeostasis (5–7). Several models to study NHE function have been generated by targeted disruption of the *nhe1*, *-2*, and *-3* genes (8–10), but compensatory responses have, in some cases, blunted the impact of Na<sup>+</sup>/H<sup>+</sup> exchanger loss-of-function. *Caenorhabditis elegans* is a simple alternative model organism with a high degree of similarity to mammals both physiologically and genetically. As the entire repertoire of nine potential Na<sup>+</sup>/H<sup>+</sup> exchanger homologs has recently been cloned from *C. elegans* (11), we have utilized a combination of reverse genetics and a novel technique for *in vivo* pH measurements to assess the role of one of these isoforms in normal gut function.

Nutrient uptake processes in absorptive epithelia such as the intestine can be coupled to inward movement of a proton and thus tied indirectly to the cellular resting pH. Although it has long been known that the rate of substrate absorption via the PepT1 and T2 oligopeptide-H<sup>+</sup> symporters is greatly enhanced at a low extracellular pH (12, 13), more recent data suggest that the resulting cytoplasmic acidification leads to the selective activation of apical Na<sup>+</sup>/H<sup>+</sup> exchangers (primarily NHE3) in intestinal Caco-2 cells (14). In addition, while this study was in progress, a report was published suggesting that the inhibition of dipeptide uptake caused by treatment with vasoactive intestinal peptide was indirect and manifest primarily through a modification of NHE3 activity (15). These results suggest that a functional coupling occurs between oligopeptide uptake and Na<sup>+</sup>/H<sup>+</sup> exchange at the apical cell membrane. However, it is not known whether these observations hold *in vivo* nor whether Na<sup>+</sup>/H<sup>+</sup> activity is required for oligopeptide uptake in a live organism.

In order to address this question, we turned to the nematode *C. elegans*. Exclusive localization of the NHX-2 isoform to the apical membrane of the intestine suggested that it might represent the nematode NHE3 ortholog. In addition, the nematode genome contains the coding potential for three H<sup>+</sup>-coupled oligopeptide transporters (*opt-1*, *-2*, and *-3*), which have been functionally expressed and shown to possess dipeptide transport activity that is enhanced by a transmembrane H<sup>+</sup> gradient (16, 17). We demonstrate here that the *opt-2* gene codes for the intestinal H<sup>+</sup>-oligopeptide symporter and suggest using a combination of reverse genetics and a novel *in vivo* pH imaging technique that the activity of OPT-2 is closely linked to the intracellular pH established specifically by NHX-2 in the nematode intestinal epithelia. Our observations are also consistent with preferential activation of the intestinal Na<sup>+</sup>/H<sup>+</sup> exchanger on the apical membrane by nutrient-induced acidification. Most importantly, our results show that an inhibition of Na<sup>+</sup>/H<sup>+</sup> exchange can lead to a phenotype resembling caloric

\* This work was supported by National Institutes of Health Grants DK062763 (to K. N.) and DE08921 and (to James E. Melvin). The costs of publication of this article were defrayed in part by the payment of page charges. This article must therefore be hereby marked "advertisement" in accordance with 18 U.S.C. Section 1734 solely to indicate this fact.

‡ To whom correspondence should be addressed: Gastroenterology Unit, Dept. of Medicine, University of Rochester Medical Center, Box 646, 601 Elmwood Ave., Rochester, NY 14642. Tel.: 585-275-5156; Fax: 585-506-1967; E-mail: keith\_nehrke@urmc.rochester.edu.

<sup>1</sup> The abbreviations used are: NHE, electroneutral Na<sup>+</sup>/H<sup>+</sup> exchanger; pH<sub>i</sub>, intracellular pH; GFP, green fluorescent protein; dsRNA, double stranded RNA; RNAi, double-stranded RNA mediated gene interference; Gly-Sar, glycylsarcosine; EIPA, 5-(*N*-ethyl-*N*-isopropyl)amiloride.

restriction, perhaps through a reduced nutrient uptake capacity, and a concomitant increase in life span.

#### MATERIALS AND METHODS

**Promoter Transgene Cloning and Strains**—Strains used were SU93, containing an integrated *ajm-1::GFP* translational fusion that labels cell boundaries in the embryo, e2131<sup>ts</sup>, containing a mutant temperature-sensitive *pha-1* allele that prevents pharyngeal development, and the wild-type N2, Bristol strain. These strains were routinely propagated at 15 °C on nematode growth media agar plates containing 5  $\mu\text{g}/\text{ml}$  cholesterol and seeded with OP50 bacteria.

The vectors pRNAi-nhx-2 and opt-2 were created by PCR cloning from nucleotide 133 to 1759 and from nucleotide 649 to 1339 of the respective coding regions into the double-stranded RNA (dsRNA) feeding vector pPD129.36. The feeding vectors pLT61.1, containing an *unc-22* insert, and pLT63.1, containing a *fem-1* insert (courtesy of A. Fire, Carnegie Institute of Washington, Baltimore, MD), were used as controls to assess the efficiency of double-stranded RNA-mediated gene interference (RNAi). Transcriptional promoter fusions to GFP were created by PCR amplification of 4 kb of genomic sequence from upstream of the first start codon for *nhx-2*, *opt-1*, and *opt-2* using restriction site-tagged oligonucleotide primers that contained a mutated start codon complement (ATG to TTG) to prevent translational initiation. The PCR products were cloned into the complementary sites of the vector pFH6.II (courtesy of F. Hagen, University of Rochester, Rochester, NY), which is a derivative of pPD 95.81 (courtesy of A. Fire, Carnegie Institute of Washington, Baltimore) to create pJP109-nhx-2, pKN109, and pKN110, respectively. Translational promoter fusions were created similarly but instead used a downstream genomic primer that annealed immediately prior to the stop codon (rather than start codon), and the PCR product was cloned so that GFP would be translated in-frame with the full protein coding regions for *nhx-2* (pJP113-nhx-2) or *opt-2* (pKN111).

To create a nematode expression vector for pHluorin, a PCR product was amplified containing the 5'-coding sequences of GFP, including the first three synthetic introns, from the vector pFH6.II (synthetic introns greatly enhance the stability of mRNA in *C. elegans*). A separate PCR product was then amplified from an expression vector for ratiometric pHluorin in pGEX-2T (courtesy of James Rothman, Sloan-Kettering Institute, New York). This product contained the 3'-coding sequences of pHluorin, including all of the pHluorin mutations, and also included a 30-nucleotide overlap at the 5' end with the 3' end of the PCR product from pFH6.II. These two PCR products were annealed, extended, and reamplified using primers to the 5'- and 3'-most sequences of the extended product. The final PCR product was used to replace GFP in a pFH6.II background. Finally, the enhanced GFP mutation (S65C) in the pFH6.II vehicle was converted back to a serine by QuikChange mutagenesis (Stratagene, La Jolla, CA). This construct represented a promoterless pHluorin expression vector with four synthetic introns (one each in the 5'- and 3'-untranslated regions) and contained the *unc-54* 3'-untranslated region. The entire coding region and four synthetic introns in the final vector pIA3 were sequenced on both strands. We found that the L220F mutation was not present in either pIA3 nor in the original pHluorin clone provided. The *nhx-2* promoter was used to drive pHluorin expression in the gut, as described (11). A nematode 4 synthetic intron expression vector for ecliptic pHluorin (18) was also engineered but was not used in this work.

**Nematode Microinjections**—GFP or pHluorin fusion constructs were mixed with pCL1, which rescues the *pha-1* deficit (19), at 75  $\mu\text{g}/\text{ml}$  each in high potassium injection buffer, and then coinjected into the gonad of young adults, as described (20). After 4 days at 22 °C, surviving F1 progeny were picked from at least 10 injections to separate plates to look for germ line transmission. F2 generation nematodes were then imaged on 2% agarose pads using either a Nikon Eclipse E800 microscope equipped with Nikon Apo series objectives under 100-watt mercury illumination and a GFP or 4,6-diamidino-2-phenylindole filter set, or a Leica DRME confocal microscope under 488-nm laser illumination and a fluorescein isothiocyanate filter set as appropriate. The images were captured using a Spot2 camera and analyzed in Adobe Photoshop (Adobe Systems, San Jose, CA).

**RNAi and Growth Analysis**—Fresh transformants of each RNAi vector, including the insertless control vector pPD129.36, were grown in the bacterial strain HT115 to mid-log phase at 37 °C and then induced for 2 h with 1 mM isopropyl- $\beta$ -D-thiogalactopyranoside. After 5-fold concentration, 80  $\mu\text{l}$  of bacteria was added to the surface of 35-mm nematode growth media agar plates supplemented with cholesterol and 0.1 mM isopropyl- $\beta$ -D-thiogalactopyranoside. Two days later, L4 larvae

were placed onto the RNAi plates for 24 h prior to being moved to a fresh plate, where they were allowed to lay eggs for a period of 12–24 h.

The maturation and phenotype of these progeny were assessed using a variety of methods. In order to measure growth rate, images of each animal were captured daily through a Nikon E800 microscope as described above. Images were stored using SPOT image software and then calibrated, measured, and transferred to Origin 6.1 (OriginLab Corp., Northampton, MA) for analysis. To determine rates of pharyngeal pumping, video was captured using a dissecting microscope fitted with a DAGE digital camera and transferred to a SONY TRV-120 digital camcorder. Playback was later slowed electronically to follow pharyngeal contractions. To assess the brood size, F1 generation nematodes were transferred to fresh RNAi plates every 24 h, and the progeny were counted and removed using a flame-drawn pipette connected to a vacuum source. Mortality of the F1 nematodes was assessed daily over a period of 5 weeks.

Nile Red staining was used to assess the distribution of fat in the RNAi-treated worms. Nile Red was diluted to 0.25  $\mu\text{g}/\text{ml}$  in M9 buffer, and 1 ml was spread and allowed to dry onto 35-mm seeded RNAi plates (final concentration 0.05  $\mu\text{g}/\text{ml}$ ). Newly hatched larva were transferred to these plates and allowed to mature. These worms were then anesthetized in M9 solution containing 0.1% tetramisole and 0.1% Tricaine and imaged on 2% agarose pads using a rhodamine filter set as described above. The overall pattern (or lack) of staining did not differ greatly between the various larval stages in the RNAi-treated samples, although the degree of fluorescence in the region of the lumen increased in *nhx-2* RNAi-treated worms as they aged.

To assess the distribution of cells in the F2 generation embryos, the SU93 strain was subjected to RNAi treatment, and the F2 embryos were examined under both fluorescent and Nomarski optics as described above.

**Intracellular pH Measurements and Dipeptide-induced Acidification**—The intestinal pH of nematodes expressing pHluorin was examined using a glue-down and perfusion technique coupled with real time fluorescent microscopy. Nematodes (L4 or young adult) were glued to 2% agarose/M9 pads on 40-mm glass coverslips using NexaBand H/C, a cyanoacrylate veterinary adhesive, and were then place into an perfusion chamber (Warner Instruments, Hamden, CT) and superfused with a nominally bicarbonate-free physiological saline solution (in mM: 135 NaCl, 5.4 KCl, 0.4  $\text{KH}_2\text{PO}_4$ , 0.33  $\text{NaH}_2\text{PO}_4$ , 20 Hepes, 1.2  $\text{CaCl}_2$ , 0.8  $\text{MgSO}_4$ , pH adjusted to 7.4 with Tris base). A dual wavelength excitation system (TILL Photonics, Germany) rigged to a Nikon E2000 inverted microscope equipped with a CCD camera detection system (Cooke, Germany) was used to monitor pH changes. The fluorescent emissions were measured at 530 nm following excitation at 410 and 470 nm. To convert the derivative fluorescent ratio to  $\text{pH}_i$ , the intestinal cells were exposed via gently slicing open the worm with a 32-gauge needle immediately posterior to the pharyngeal-intestinal valve, and *in situ* calibration was performed using the high  $\text{K}^+$ /nigericin technique (21). For experiments where pH was followed over time, pharyngeal pumping was initiated by the addition of serotonin to 2 mM final concentration, and all subsequent solutions contained serotonin. To assess oligopeptide-induced acidification, the superfusate was first switched to sodium-free solution containing NMDG/HCl in place of NaCl, and after several minutes, the dipeptide glycylsarcosine (Gly-Sar) was added to a final concentration of 20 mM. Recovery from acidification was then monitored in the original salt solution, plus or minus the addition of 5-(*N*-ethyl-*N*-isopropyl)amiloride (EIPA).

#### RESULTS

**NHX-2 Protein Colocalizes with OPT-2, an Intestinal  $\text{H}^+$ -Oligopeptide Transporter**—GFP reporter constructs that expressed transcriptional or translational promoter fusions in transgenic nematodes were used to assess cellular expression patterns and protein distributions of candidate genes that may represent nematode orthologs of the mammalian NHE3 and PepT1 proteins. We have shown previously (11) that NHX-2 is expressed strongly and uniformly throughout the apical membrane of intestinal cells, making it a likely candidate for the mammalian NHE3 ortholog. Those results were confirmed in Fig. 1 (panels A, B, G, and H). In addition, *C. elegans* has three genes that could represent the mammalian PepT1  $\text{H}^+$ -coupled oligopeptide transporter ortholog, named *opt-1*, *-2* and *-3*. Although all three genes code for functional transporters (16, 17), *opt-3* is expressed in a pan-neural pattern (16), making it an

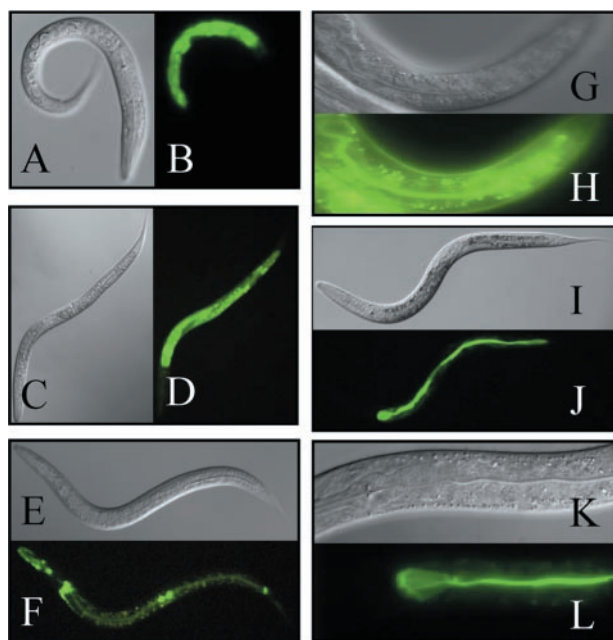


**FIG. 1. Expression patterns for NHX-2, a sodium-proton exchanger, and OPT-2, a proton-coupled oligopeptide transporter, using promoter::GFP transgenic reporter strains.** GFP reporter expression in transgenic nematodes was driven by genomic DNA fragments containing either 4 kb of promoter alone (panels A–F) or 4 kb of promoter along with the entire open reading frame of the cognate protein, fused in-frame with GFP (panels G–L). The *nhx-2* gene promoter (panels A and B) and the *opt-2* gene promoter (panels C and D) drove GFP expression in the gut of the worm. The *opt-1* gene promoter caused GFP to be expressed primarily in pharyngeal and vulval regions (panels E and F). The NHX-2 (panels G and H) and the OPT-2 (panels I–L) fusion proteins were targeted to the apical membrane of the intestine, which expands prior to contacting the pharynx, as demonstrated in panel L.

unlikely candidate to interact with NHX-2. Similarly, the *opt-1* promoter drove GFP expression in a variety of cells, including vulval, pharyngeal, and anal muscles but not in the intestine (Fig. 1, panels C and D). However, the *opt-2* gene promoter drove GFP expression specifically in the intestine (Fig. 1, panels C and D), and the OPT-2::GFP fusion protein was distributed along the apical membrane of the intestinal cells, coincident with the NHX-2::GFP fusion (panels I–L).

**RNAi of *nhx-2* and *opt-2* Results in Both Overlapping and Distinct Phenotypes**—The role of the *nhx-2* and *opt-2* gene products in nematode development was studied using double-stranded RNA-mediated gene inactivation, which phenocopies a loss-of-function null allele. dsRNA was introduced via bacterial feeding (22, 23), which is particularly potent in intestinal cells. Fig. 2 shows 2-day-old worms grown on *Escherichia coli* expressing dsRNA from insertless control, *opt-2*, or *nhx-2* vectors (panels A–C, respectively). It is immediately apparent that both *opt-2* and *nhx-2* are required for optimal growth, as the RNAi-treated worms are shorter, thinner, and more transparent relative to the representative control worm. This decreased opacity is quite likely related to the accumulation of fat storage granules in the intestine. A recent report (24) on fat regulatory genes in *C. elegans* in fact demonstrated that RNAi inactivation of *opt-2* caused a reduction in fat content, as assessed by Nile Red staining. We found this to be true in our work as well (Fig. 3, panels A–D) but not to the same extent as *nhx-2* gene inactivation, which resulted in a nearly complete loss of fat storage granules in the intestine (Fig. 3, panels E–H). This is consistent with the smaller size of the worms following *nhx-2* gene inactivation (Fig. 2). Confocal microscopy using a longer exposure time revealed that much of the residual Nile Red

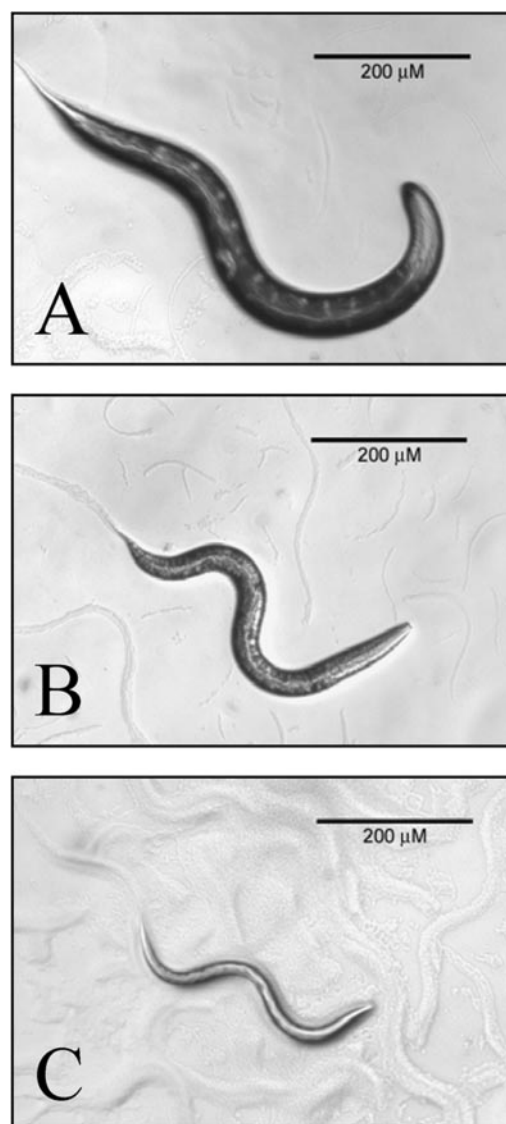


**FIG. 2. Transmission micrographs of control, *nhx-2*, and *opt-2* RNAi-treated nematodes 48 h post-hatching.** Double-stranded RNA was induced in bacteria and administered using a feeding method to L4 stage animals for 24 h. Those animals were then allowed to lay ~50 eggs on fresh RNAi plates before being removed. The eggs (F1 progeny) were allowed to develop and then scored for phenotype. At 48 h post-hatch, the control F1 nematodes (panel A) appeared normal and healthy, whereas the *opt-2* and *nhx-2* RNAi-treated nematodes (panels B and C, respectively) were small (*gro* phenotype), appeared transparent (*clr* phenotype), and lagged behind the control nematodes in larval maturation as well. Both the *opt-2* and *nhx-2* nematodes gross morphology appeared normal, however.

staining following *nhx-2* gene inactivation occurred in the lumen of the intestine (panels G and H). This may represent a deficit in transport of receptor-bound substrates for Nile Red staining or perhaps a weak signal that is normally veiled by the intense staining of the gut granules.

A more complete analysis of several physiological indicators of the metabolic state following gene inactivation is shown in Fig. 4. Quantitative growth curves for the RNAi-treated worms indicate that both the rate of growth and the final size is impaired by abolition of either gene product or by both in combination (Fig. 4, panel A), a fact that suggests they function in the same physiological pathway. In addition, progression through the four larval stages, particularly the L1/L2 stages, is also slowed by RNAi treatment (data not shown). The rate of pharyngeal pumping was slower in *nhx-2* RNAi-treated worms

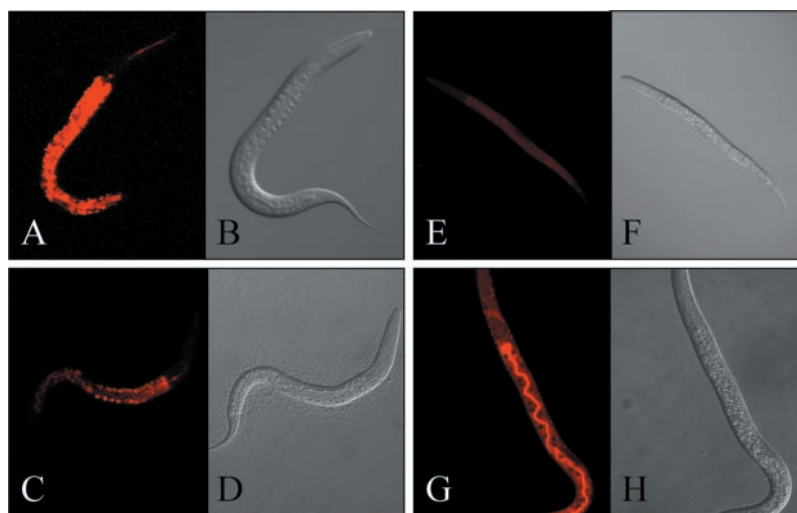


FIG. 3. **Changes in fat content in RNAi-treated nematodes.** Nile Red was added to NGM plates containing bacteria expressing control dsRNA (panels A and B) and dsRNA targeted toward *opt-2* (panels C and D) or toward *nhx-2* (panels E–H). L4 nematodes were seeded onto untreated RNAi plates for 24 h prior to being moved to plates containing Nile Red. The F1 progeny were allowed to grow for 48–96 h following hatching on Nile Red plates. These progeny were examined by fluorescence microscopy under a rhodamine filter set (panels A, C, E, and G) and under a DIC filter set using transmitted light (panels B, D, F, and H). Control nematodes stained brightly in presumed lipid storage granules in the intestine (panel A), as reported previously (24). Under identical exposure conditions, *opt-2* gene inactivation resulted in a dramatic decrease in fluorescent intensity (panel C), whereas *nhx-2* gene inactivation resulted in a nearly complete loss of fluorescence in the gut granules (panel E), reflecting a lower level of fat accumulation in the intestine. By using confocal microscopy and a longer exposure, the majority of Nile Red staining was observed at the luminal surface of the intestine following *nhx-2* gene inactivation (panel G).

than in control worms ( $p < 0.01$ ). However, there was no apparent difference between the *opt-2* RNAi-treated and control worms (Fig. 4, panel B). Likewise, the brood size was severely reduced from ~200 to 300 progeny in the control to less than 5 progeny in the *nhx-2*-treated worms but was only reduced by 2-fold in the *opt-2*-treated worms (Fig. 4, panel C). Finally, the life span of the worms was assessed, and the percent survival was plotted on a daily basis over the course of 5 weeks (Fig. 4, panel D). On average, *nhx-2* RNAi treatment caused an increase of 30–40% in post-reproductive life span, consistent with previous models of nutrient deprivation (25–27). In fact, caloric restriction has been shown in worms to lead to many of the same phenotypes observed in our *nhx-2* gene inactivation model, *i.e.* an increase in the average life span, decreased brood size, and reduced accumulations of lipid storage granules in the intestine (28). Mutations in a variety of genes involved predominantly in pharyngeal function and, correspondingly, food uptake mirrors these phenotypes (29). Caloric restriction can also lead to an increased life span in mammals, suggesting that many of the physiological changes that occur from restricted dietary intake are conserved along the evolutionary scale (30, 31).

The mean life span of the *opt-2* RNAi-treated worms also increased by several days, but this small effect may reflect the observed delay in larval maturation and not an increase in post-reproductive life span at all. Finally, the slight reduction in life span of the double RNAi-treated animals compared with the *nhx-2*-treated animals may represent a dosage effect of mixing dsRNAs that appears over time; note that the initial rates of die-off appear similar, and differences begin to arise after about 50% of the worms have perished. These data suggest that whereas NHX-2 may facilitate dipeptide uptake by OPT-2, as the combined effects of inactivating both genes was no more detrimental than NHX-2 alone, they also suggest that NHX-2 is involved in other aspects of intestinal function that result in severe physiological consequences.

To examine more closely the reason behind the reduced brood size in the RNAi-treated worms, embryogenesis was examined in the F2 generation using the SU93 strain, which expresses an adherin::GFP fusion protein that labels cell

boundaries. The control and *opt-2*-treated F2 embryos appeared to develop normally (Fig. 5, panels A–D), whereas the few *nhx-2*-treated embryos that were laid were morphologically abnormal (panels E and F). It is unlikely, however, that *nhx-2* plays a direct role in embryonic development, as the F1 embryos appeared normal and the F1 brood was of a comparable size with control worms (data not shown). In addition, we have not observed *nhx-2*::GFP reporter expression prior to the L1 larval stage (11). Instead, we hypothesize that the embryos are not getting enough nutrients to develop normally in the absence of maternal NHX-2 activity.

From these results, we conclude that whereas the *nhx-2* gene product may in fact be functionally coupled to the activity of OPT-2 in the intestine, there is potentially an additional unexplored role for intestinal  $\text{Na}^+/\text{H}^+$  exchange in other nutrient uptake processes, particularly those involved in regulating fat accumulation and storage, and loss of this function results in worms that display a phenotype mirroring starvation.

**NHX-2 Sustains the Normal Resting  $\text{pH}_i$  of Intestinal Cells**—To assess more directly the role of intestinal  $\text{Na}^+/\text{H}^+$  exchange in promoting  $\text{H}^+$ -coupled oligopeptide uptake, a model was established to measure the  $\text{pH}_i$  of intestinal cells in living worms under physiological conditions, such as following exposure to dipeptide substrate. The basis of this model relied upon pHluorin, a pH-sensitive mutant of GFP (18). pHluorin has been used to assess pH changes following synaptic transmission and endocytotic vesicle fusion (18, 32) in organelles of the secretory pathway (33) and in peroxisomes (34). A line of transgenic worms was established that expressed the ratiometric variant of pHluorin in intestinal cells using the *nhx-2* promoter. Signal errors caused by variations in concentration, path length, leakage, and photobleaching are greatly reduced with ratiometric imaging methods and, as Fig. 6 demonstrates, the variation in single wavelength intensity was greater than the variation in the 410/470 nm fluorescent excitation ratio (panels A–F). The ability to perform ratiometric pH measurements with millisecond resolution was critical to our experiments, as the worms could not be paralyzed under our experimental conditions and moved slightly during imaging.

To demonstrate that the observed ratios accurately reflected

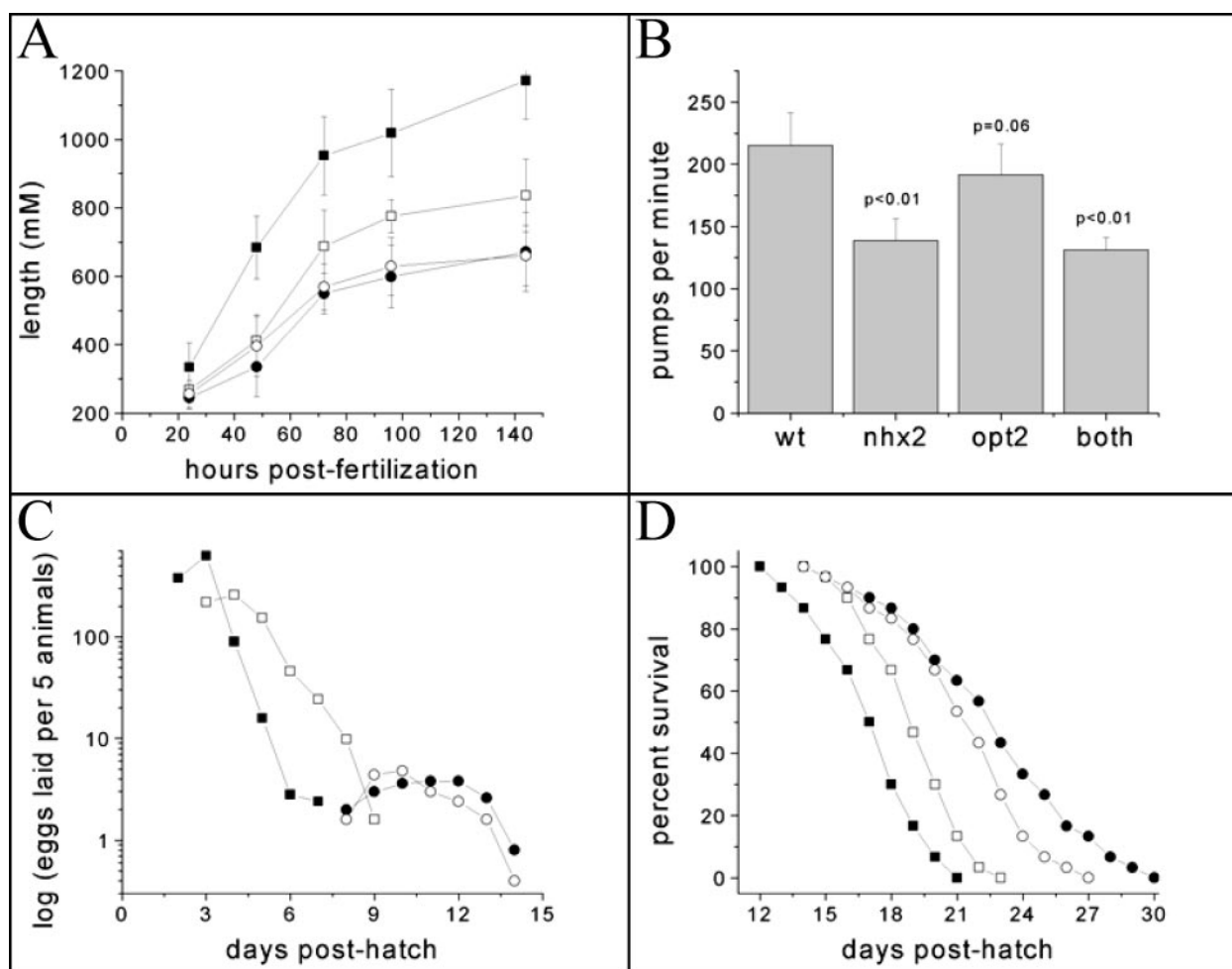


FIG. 4. Physiological changes reflecting starvation are associated with the loss of NHX-2. The effects of RNAi targeting of *opt-2* (□), *nhx-2* (●), or both *opt-2* and *nhx-2* together (○) were compared with control RNAi (■) on four key indicators of nutrient availability. Panel A, F1 generation nematodes ( $n = 40$ ) were scored for size at 24-h periods following hatching. In addition to being smaller, the *nhx-2* and *opt-2* RNAi-treated worms took several days longer than the control for larval maturation to progress to adulthood (data not shown). Panel B, pharyngeal pumping was measured using video capture in adult F1 generation nematodes (72 h post-fertilization for control and 120 h post-fertilization for *opt-2* and *nhx-2*). Although the rate of pharyngeal pumping was lower in the *opt-2* RNAi-treated worms, the difference was not statistically significant ( $p = 0.06$ ). Panel C, brood size of the F1 generation was assessed ( $n = 25$ , 5 plates with 5 worms apiece) by counting F2 progeny at 24-h time points and moving the adults to new plates. The *nhx-2* RNAi-treated F1 generation was essentially sterile, whereas the *opt-2* worms had a reduced brood size. Panel D, life span determinations were performed at 22 °C on the F1 generation nematodes ( $n = 30$ ). Whereas the *opt-2* RNAi-treated worms appeared to survive on average several days longer than the control, the rate of die-off was similar, which may reflect the observed delay in maturation rather than an increase in longevity (see text). The loss of *nhx-2*, however, resulted in a dramatic 40–50% increase in the life span, which is consistent with the effects of nutrient deprivation in the nematode model.

the intracellular pH, a calibration curve was generated using the high  $\text{K}^+$ /nigericin technique, where  $\text{pH}_i = \text{pH}_o$  (21). L4/early adult nematodes were glued to an M9/2% agarose pad using Nexaband H/C, as described previously (35). A small slit was made immediately posterior to the pharynx, whereupon the intestine extruded through the slit and was bathed in buffers of differing pH. A plot of the emission ratio at 540 nm following dual excitation at 410/470 nm versus the  $\text{pH}_o$  was then fit to a Boltzmann equation (Fig. 6G), and subsequent ratiometric measurements were converted to  $\text{pH}_i$  using the calibration curve.

Initially intestinal cell  $\text{pH}_i$  was determined as a function of both age and following gene inactivation. We noted that there was small but statistically significant difference between young L1/L2 larva and adults ( $\text{pH} 7.48$  versus  $7.6$  ( $p < 0.05$ )). Thus, to minimize age-dependent variation, subsequent experiments used exclusively L4 larva and early adults. The  $\text{pH}_i$  of worms fed *nhx-2* dsRNA ( $7.23 \pm 0.10$ ) was significantly lower than the  $\text{pH}_i$  of control animals ( $7.53 \pm 0.07$  ( $p < 0.01$ )), indicating that the NHX-2 protein plays a role in establishing the normal resting  $\text{pH}_i$  in intestinal epithelial cells. This result suggested

that the contributions of other NHX isoforms in the intestine to maintenance of a high resting  $\text{pH}_i$  was minimal at  $\text{pH}_i$  values above 7.2; this may reflect the internal “set point” of these exchangers, as determined by the intracellular proton-binding sites and/or interacting proteins or modifications. Gene inactivation of *opt-2* alone did not result in an appreciable shift in intestinal pH ( $7.51 \pm 0.07$ , ( $p = 0.38$ )), whereas inactivation of both *opt-2* and *nhx-2* together resulted in a slightly more acidic intestinal resting pH compared with *nhx-2* alone ( $7.20 \pm 0.09$ ). Thus the OPT-2 protein, despite normally transporting a proton along with oligopeptide substrate, does not by its absence affect intestinal pH homeostasis.

**OPT-2-dependent Acidification and Recovery Mediated by the NHX-2 Exchanger**—In order to establish the role of NHX-2 and OPT-2 proteins in regulating intestinal pH under conditions where OPT-2 is more likely to be active, *i.e.* in the presence of dipeptide substrate, worms were glued down and superfused with a physiological media containing Gly-Sar, a model substrate for  $\text{H}^+$ -coupled oligopeptide transporters, both in the presence and in the absence of sodium. Serotonin was used to initiate pharyngeal pumping after the worms had been glued

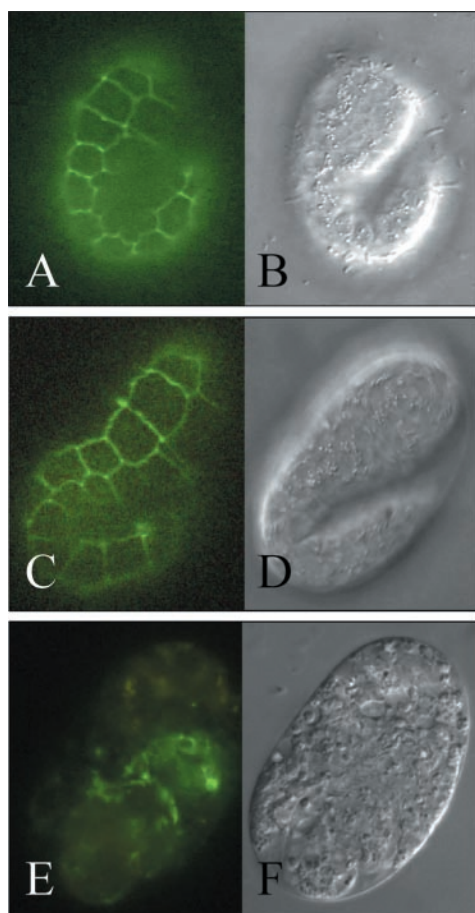


**FIG. 5. The reduced brood size associated with the loss of NHX-2 reflects a general morphological disorganization of the F2 embryo.** A nematode strain containing an integrated transgene that expresses an adherin::GFP translational fusion product (*ajm1*) in the embryo was exposed to control (panels A and B), *opt-2* (panels C and D), or *nhx-2* (panels E and F) dsRNA. Embryos from the F2 generation were examined at approximately the same stage of development using fluorescent microscopy under a GFP filter (panels A, C, and E) or DIC optics (panels B, D, and F). The cell junctions were clearly defined in the control and *opt-2* RNAi-treated embryos, whereas the *nhx-2* embryos were morphologically disorganized and contained large vacuoles, as can be seen in the DIC micrograph. These embryos were unviable and eventually became entirely infused with vacuoles.

down. In this system, pharyngeal pumping is required to maintain fluid movement through the intestine and to allow the introduction or removal of substrates from the intestinal ion transport proteins. Despite a report that sodium is required for establishing an action potential in the pharynx (36), we found that pharyngeal pumping persisted following the removal of sodium from the perfusate. This may reflect a requirement for sodium at the basolateral surface of the pharynx, which would not be exposed to the superfusate and might be more slowly depleted of sodium. Correspondingly, in the absence of pharyngeal pumping, the pH changes reported below upon switching solutions were dramatically blunted. Thus, all of the nematodes were required to exhibit strong (>60 pumps/min) pharyngeal pumping at the initiation and conclusion of each experimental run.

Fig. 7 shows the results of sodium-depletion and/or dipeptide addition on intestinal cell  $\text{pH}_i$  in control and *opt-2* or *nhx-2* RNAi-treated worms. It is important to note that the worms were incubated in physiological saline solution for at least 15 min prior to analysis, so as to minimize the influence of exogenous substrates derived from leftover food in the intestine. In general, the experimental protocol called for the addition of

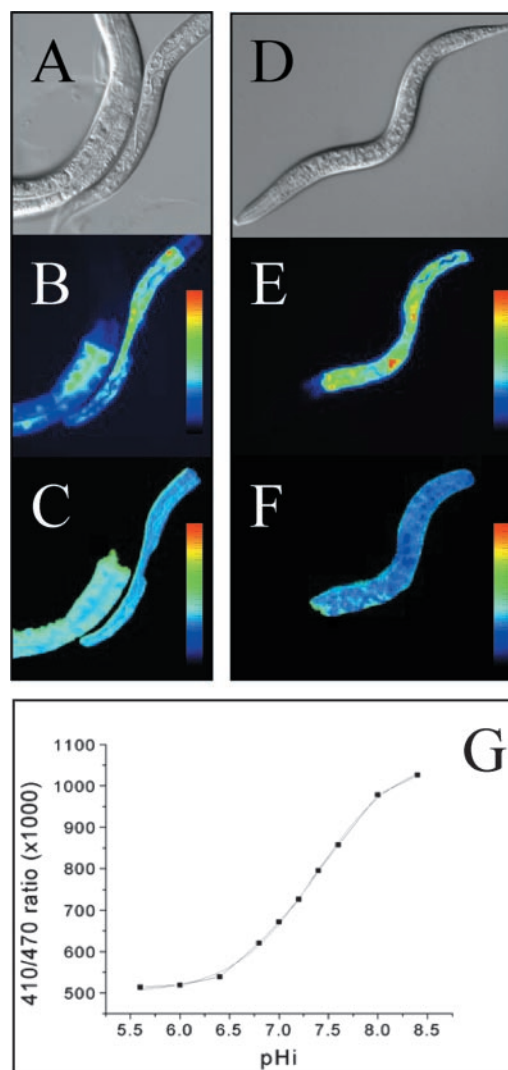


**FIG. 6. A genetically encoded pH indicator demonstrates a role for NHX-2 in maintaining the resting pH of intestinal cells.** pHLuorin is a pH-sensitive GFP mutant isoform with a defined isosbestic point (410 nm) that is useful for ratiometric fluorescent measurement of intracellular pH, particularly in a transparent organism such as *C. elegans*. A construct containing the pHLuorin coding region, interrupted by four synthetic introns and driven by the *nhx-2* promoter, was injected into nematodes to create a transgenic strain for measuring the pH of the intestine. The nematodes were anesthetized in M9 media on an agarose pad, and pHLuorin was excited at dual wavelengths of 410 and 470 nm; emissions were measured at 530 nm. DIC (panels A and D), fluorescence (panels B and E; excitation at 470 nm, emission at 530 nm), and dual excitation ratio images (excitation at 410/470 nm, emission at 530 nm) for control (panels A–C) and *nhx-2* RNAi-treated nematodes (panels D–F) demonstrate that the 410/470 nm fluorescence ratio is independent of expression levels of pHLuorin. Pseudocolor scale bars are shown in the lower left of each panel; scaling was fitted linearly to the entire signal range in each image. An *in situ* high potassium/nigericin calibration of pHLuorin using transgenic nematodes that had been cut open immediately posterior to the pharynx generated a curve that is best fit by the Boltzmann equation  $y = (A_1 - A_2)/(1 + e^{(x-x_0)/dx}) + A_2$ , where  $A_1 = 501$ ,  $A_2 = 1073$ ,  $x_0 = 7.37$ , and  $dx = 0.413$  (panel G). This equation was then used to calculate pH from the experimentally determined 410/470 ratios.

serotonin to a normal physiological saline superfusate at time 0. The intestinal cell  $\text{pH}_i$  was followed for 5 min, at which point sodium was reduced in the superfusate to nominal levels. After an additional 10 min, dipeptide substrate was added. Finally, after 30 min of exposure to dipeptide, sodium was added back to the solution, and the dipeptide was removed.

Incubation of control nematodes in the absence of sodium

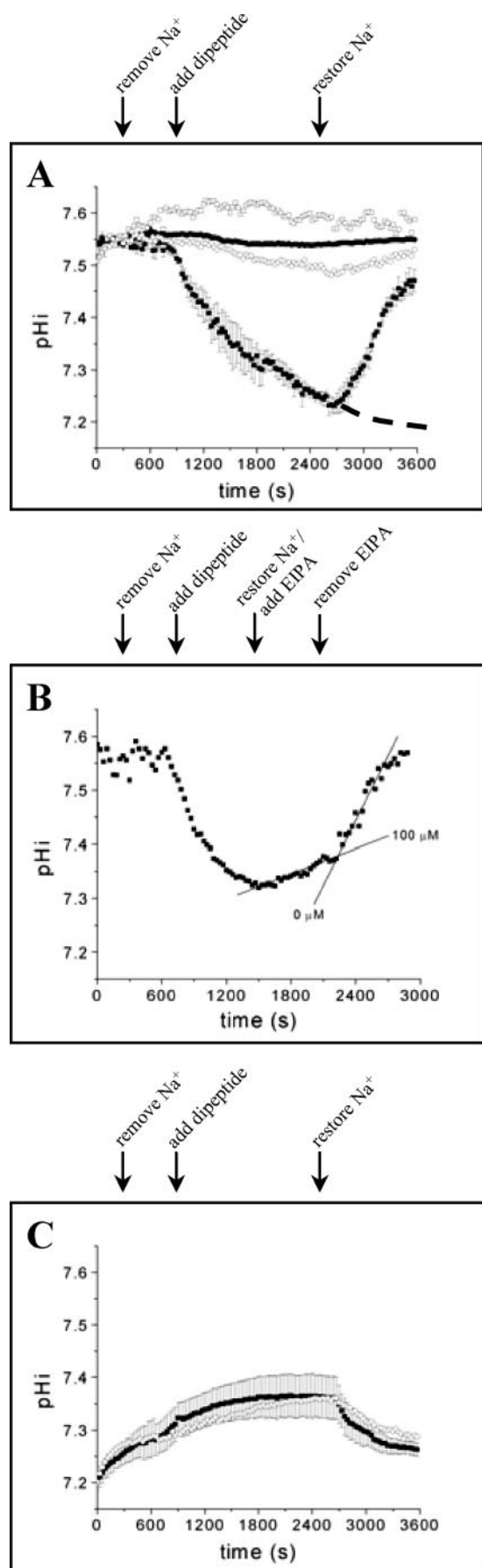


FIG. 7. NHX-2 activity is physiologically coupled to oligopeptide uptake via OPT-2 at the intestinal luminal membrane. A glue-down technique was used to immobilize live worms expressing

elicited almost no change in the intestinal  $\text{pH}_i$  over the course of the experiment in the representative trace shown in Fig. 7, panel A (filled circles). Although this condition might be expected to mimic the effect of *nhx-2* gene knockdown, the lack of acidification suggests that either a recovery mechanism is in place that does not rely on luminal sodium or that the forces driving acidification are not present in the absence of food. It is important to remember that the basolateral surface of the intestinal cells is bathed by the pseudocoelomic fluid, which presumably contains  $\text{Na}^+$ , and so the effects we observed are not necessarily what would be seen in isolated cells or cells in culture, for example. In contrast, the addition of dipeptide in the absence of sodium led to a slow intracellular acidification (Fig. 7, panel A, filled squares,  $n = 3$ ). Persistent exposure to dipeptide in the absence of sodium demonstrated that acidification stopped once the  $\text{pH}_i$  reached 7.2 (Fig. 7, panel A, dashed line). The acidification appeared to be entirely due to the activity of the OPT-2 protein, as gene inactivation of *opt-2* prevented dipeptide-induced acidification (Fig. 7, panel A, open squares). The re-addition of sodium at 2400 s allowed the  $\text{pH}_i$  to recover to normal resting levels, whereas EIPA blunted the rate of  $\text{pH}_i$  recovery (Fig. 7, panel B). This, together with the observation that EIPA promoted dipeptide-induced acidification even in the presence of  $\text{Na}^+$  (data not shown), demonstrates the homeostatic role of  $\text{Na}^+/\text{H}^+$  exchange in maintaining the normally high resting  $\text{pH}_i$ . These results indicate that OPT-2 is the primary means of dipeptide transport into the intestinal epithelia and that failure to buffer this activity via a sodium-dependent, EIPA-sensitive  $\text{pH}$  regulatory activity leads to acidification to a new resting state. The final steady-state resting  $\text{pH}_i$  of cells that occurred in the absence of  $\text{Na}^+$  was similar to the resting  $\text{pH}_i$  of cells following *nhx-2* gene inactivation, suggesting that NHX-2 activity specifically is critical between  $\text{pH}_i$  of 7.2 and 7.6 for  $\text{pH}$  homeostasis.

Intestinal cell  $\text{pH}_i$  as a function of dipeptide uptake was examined following *nhx-2* gene inactivation as well (Fig. 7, panel C). The resting  $\text{pH}_i$  of the NHX-2-deplete cells was at or

intestinal pHluorin. The worms were superfused with a physiological salt solution, and serotonin was added to stimulate pharyngeal pumping. Following the onset of pumping, 410/470 ratiometric images of the intestine were obtained. The resulting data were then converted to  $\text{pH}$  and plotted versus time. Panel A, the nematodes were switched to a sodium-free solution at time 1 (300 s), as indicated. Ten minutes later, at time 2 (900 s), the dipeptide Gly-Sar was added to provide a model substrate for proton-oligopeptide symport. Finally, at time 3 (2700 s), as indicated by the 3rd arrow, sodium was added back, and the dipeptide was removed. In the case of the control nematodes ( $\blacksquare$ ,  $n = 4$ ), the addition of Gly-Sar caused an intracellular acidification from  $\sim 7.55$  to 7.25 over 30 min that was reversible upon the re-addition of sodium to the apical surface. The dashed line represents the result when sodium is not added back to the worm; the  $\text{pH}_i$  does not decrease beyond 7.2, even with extended incubations in sodium-free media. Representative traces demonstrate that this acidification depended entirely upon the *opt-2* gene product ( $\square$ ) and was not observed in the absence of dipeptide addition ( $\bullet$ ). However, some slight acidification was caused by the addition of dipeptide even in the presence of sodium ( $\circ$ ). Panel B, a representative trace demonstrates that  $\text{Na}^+$ -dependent recovery from acidification was EIPA-sensitive, with over 75% inhibition occurring at 100  $\mu\text{M}$ , suggestive of  $\text{Na}^+/\text{H}^+$  exchange. Panel C, the *nhx-2* RNAi-treated nematodes were subject to superfusate changes as indicated above. As shown in Fig. 6, the resting  $\text{pH}$  was  $\sim 7.2$ , which increased to about 7.35 following the addition of serotonin and sodium removal ( $n = 6$ ). The addition of serotonin alone caused a slight alkaline shift in resting  $\text{pH}$ , particularly in the *nhx-2*-treated nematodes, as can be seen clearly during the first 5 min of incubation, as well as in the difference between the initial and final resting  $\text{pH}$  values. The addition of Gly-Sar had almost no effect on the  $\text{pH}_i$  of the *nhx-2* worms, as a representative trace performed under sodium-free conditions but in the absence of Gly-Sar indicates ( $\circ$ ). Instead, the alkalization was due mainly to the removal of sodium, and the re-addition of sodium caused a reversal to a more acidic resting value of 7.25.

near 7.2 prior to serotonin addition (*solid squares*), coincident with the  $\text{pH}_i$  at which a new resting equilibrium appeared to be established following dipeptide-induced acidification in control worms (Fig. 7, *panel A*). The addition of serotonin caused an increase in the intestinal cell resting  $\text{pH}_i$  (Fig. 7, *panel C*), which was also observable, but to a much lesser degree, in the control worms (Fig. 7, *panel A*). We initially hypothesized that the addition of dipeptide would not result in any (observable) reduction in  $\text{pH}_i$ , due to the same reasons that the  $\text{pH}_i$  did not go below 7.2 in the control (see "Discussion"). Indeed, this was the case, but contrary to our expectations the removal of sodium led to an increase in the  $\text{pH}_i$  of intestinal cells (Fig. 7, *panel C*, *filled squares*,  $n = 4$ ) that was not related to the addition of dipeptide (*open circles*, representative trace). It appeared unlikely that the cells had become leaky, as re-addition of sodium led to a subsequent decrease in the  $\text{pH}_i$  (Fig. 7, *panel C*). These unexpected and to date unexplained results highlight the exciting prospects of working with a whole animal model system and will undoubtedly be a subject for future investigation.

Given these results, we conclude that  $\text{Na}^+/\text{H}^+$  exchange and  $\text{H}^+$ -oligopeptide cotransport do not appear to be obligatorily coupled, as demonstrated by the robust dipeptide-induced acidification in the control worms in the absence of sodium. Instead, they appear to be functionally coupled, and the absence of dipeptide-induced acidification following *nhx-2* gene inactivation, as well as the lack of acidification in the control nematodes beyond a pH of 7.2, strongly suggests that the normally high resting pH established by the NHX-2 protein is required for optimal steady-state OPT-2 activity, such as might occur during active feeding. In addition, given the apparently high set point of the NHX-2 exchanger, we can reasonably conclude that it will be preferentially activated under physiological conditions, such as following dipeptide-induced acidification.

#### DISCUSSION

Historically, research involving membrane ion transporters has occurred primarily via the study of cell culture, cell preparations, or tissue isolated *ex vivo*. More recently, our knowledge of the biological role of these transporters has been greatly enhanced by the ability to generate mice containing targeted deletions in genes coding for ion transport proteins. In general, however, even with gene-targeted mouse models, the physiology of ion transport in higher eukaryotes has been studied outside of the living organism. The nematode *C. elegans* provides a useful alternative for studying the physiology of ion transport simultaneously at both the molecular and the systems levels, with several clear advantages over mammalian systems. First, the ability to use genetics and reverse-genetics to quickly define the components of transport pathways provides a powerful means of analyzing both function and regulation. Second, the gene expression profiles of ion transport proteins can be determined easily via promoter::GFP fusions. Finally, because *C. elegans* is transparent, fluorescence-based methods for measuring ion flux can theoretically be used *in vivo*. This can provide a means to couple behavior, such as stimuli response, or other whole organism-specific processes directly with measurements of ion transport.

Several groups have begun to explore this possibility by expressing a fluorescent genetically encoded calcium sensor or chameleon protein in nematodes to study the role of calcium signaling in pharyngeal pumping, neuronal response to stimuli, and fertilization (35, 37). In this work, we have adopted a similar approach with a different goal; we have expressed a pH-sensitive variant of GFP in the nematode intestinal cells to establish the role of  $\text{Na}^+/\text{H}^+$  exchange in promoting nutrient and particularly dipeptide absorption in the intestine. Our

results suggest an indirect coupling between  $\text{Na}^+/\text{H}^+$  exchange and  $\text{H}^+$ -oligopeptide cotransport, with direct physiological consequences for the organism. The loss of a particular  $\text{Na}^+/\text{H}^+$  exchanger expressed on the apical membrane of intestinal cells leads to a phenotype resembling starvation and an increased life span, likely due to caloric restriction.

Although the methodology by which we address this problem is novel, the concept itself is not. Previous studies have clearly demonstrated that dipeptide transport across an epithelial cell surface is influenced by the both extracellular pH and the transmembrane  $\text{H}^+$  electrochemical gradient (for a recent review see Ref. 38). What has been less clear is why transport via endogenous  $\text{H}^+$ -oligopeptide symporters exhibits variable dependence upon extracellular sodium, whereas studies using recombinant transporters expressed exogenously indicate that sodium is not required for  $\text{H}^+$  gradient-driven dipeptide uptake (12, 39). A recent series of elegant experiments has demonstrated that the apparent sodium dependence of the endogenous symporter activity in Caco-2 tissue culture cells is due to a functional coupling between  $\text{Na}^+/\text{H}^+$  exchange and oligopeptide uptake (40, 41), and that this coupling occurs specifically with an exchanger located on the apical membrane (14). The importance of our work in relation to the previously established findings lies in the fact that we have shown that functional coupling likely occurs in live animals as well as in isolated cell systems with dramatic physiological consequences.

One of these consequences is starvation. Each of these transport proteins, which are coexpressed at the apical membrane of intestinal cells, is apparently important for fat accumulation in the intestine, and the loss of either NHX-2 or OPT-2 led to slow maturation and, in the case of NHX-2, a starvation phenotype. Similar phenotypic effects can be observed following the removal of cholesterol from the growth media or by limiting food intake (42–44). In *Drosophila*, a carboxylic acid transporter (INDY) has been shown to affect longevity, and loss of this gene also results in a caloric restriction phenotype (45, 46). Gene interference assays using the *C. elegans* dicarboxylic acid transporter orthologs demonstrate similar effects (47). These observations are consistent with a decreased availability of dicarboxylates for cellular production of metabolic energy, leading to a biological state similar to starvation, and suggest a direct role for the transporter in substrate absorption. However, in the case of NHX-2, the starvation phenotype likely arises via indirect means, as  $\text{Na}^+/\text{H}^+$  exchangers have not been shown to transport metabolic intermediates directly. We speculate here that the more severe phenotype observed with NHX-2 is due to a role for  $\text{Na}^+/\text{H}^+$  exchange or intracellular pH homeostasis in facilitating a variety of proton-coupled nutrient uptake pathways, presumably including oligopeptide absorption, although it remains possible that the reduction in intracellular pH (from 7.6 to 7.2) could perturb additional unrelated processes.

To strengthen this suggestion, we have investigated the interplay between NHX-2 and OPT-2 using a combination of RNAi and conventional physiology. Intestinal cell  $\text{pH}_i$  was determined using real time fluorescent imaging of a strain expressing pHluorin, a pH-sensitive isoform of GFP (18). Because dipeptide uptake by OPT-2 is obligatorily coupled to the influx of a  $\text{H}^+$ , we reasoned that changes in  $\text{pH}_i$  might be useful as an indirect measure of  $\text{H}^+$ -oligopeptide symport. We demonstrated initially that NHX-2 was essential for maintaining a high resting  $\text{pH}_i$  in the intestinal cells, which likely promoted dipeptide absorption via a favorable transmembrane proton gradient. We then demonstrated that dipeptide exposure in the absence of sodium resulted in acidification of the intestinal cells, consistent with cotransport of dipeptide and a proton via

OPT-2. RNAi was used to show that OPT-2 was uniquely responsible for the dipeptide-induced acidification, and we showed pharmacologically that recovery from acidification occurred primarily via Na<sup>+</sup>/H<sup>+</sup> exchange and likely through the activity of NHX-2.

It is clear from these data that Na<sup>+</sup>/H<sup>+</sup> exchange and H<sup>+</sup>-oligopeptide symport exert opposable influences on the intestinal cell pH<sub>i</sub> and that OPT-2 and NHX-2 are the proteins responsible for these activities. What remains unclear, however, is whether the rate of pH change (or lack of change) that we measured truly reflects OPT-2 activity. For example, H<sup>+</sup>-loading via dipeptide uptake at low pH<sub>i</sub> may be buffered by an alternative mechanism and/or exchanger. Thus, even though prolonged exposure to dipeptide fails to reduce the pH<sub>i</sub> of the intestinal cells beyond a value of 7.2, it remains entirely possible that a further reduction in pH<sub>i</sub> activates a Na<sup>+</sup>/H<sup>+</sup> exchanger located at the basolateral cell surface, which would have access to Na<sup>+</sup> via the pseudocoelomic fluid. Under those conditions, dipeptide uptake could occur without a concomitant change in pH<sub>i</sub> (although presumably at a lower rate due to a lesser driving force). Therefore, we are unable to demonstrate directly that oligopeptide absorption requires (or is even influenced by) the activity of a Na<sup>+</sup>/H<sup>+</sup> exchanger. However, the overlapping phenotypes and similar pH<sub>i</sub> following either dipeptide uptake or *nhx-2* gene inactivation hint strongly that OPT-2 may require NHX-2 in order to function optimally. This scenario may help to explain why the initial rate of dipeptide transport both in Caco-2 (41) and guinea pig ileum (48, 49) is Na<sup>+</sup>-independent but that the rate of transport is markedly reduced during sustained absorption in the absence of apical Na<sup>+</sup>. In addition, it would be consistent with the similar phenotypes of OPT-2 and NHX-2 following gene inactivation. Our initial attempts to measure dipeptide uptake directly were thwarted by the dissimilar sizes of the RNAi-treated worms, as well as apparently multiple dipeptide uptake pathways in cells other than the intestine that lead to background (data not shown). In addition, to date fluorescent dipeptide substrates have not been used successfully with PepT1 type cotransporters. The development of a novel fluorescent dipeptide substrate that is transported by OPT-2 would help to clarify this issue.

Our observations lead us to ask whether, in general, apical Na<sup>+</sup>/H<sup>+</sup> exchangers that are involved in mediating H<sup>+</sup> gradient-driven nutrient uptake processes will have a set point that is higher than the basolateral exchangers. Conflicting data exist with respect to this question. Expression of mammalian NHE3 leads to a higher resting pH<sub>i</sub> in the Na<sup>+</sup>/H<sup>+</sup> exchanger-deficient cell line PS120 than does expression of the basolateral housekeeping isoform NHE1 (50), and NHE3 has been shown to become maximally active at a higher pH<sub>i</sub> than NHE1 in a recombinant expression system (51). On the other hand, NHE3 has also been suggested to have a lesser affinity for H<sup>+</sup> than NHE1 (52). It is hard to determine how applicable these data may be to native proteins, however, as they have been generated using recombinant expression systems and may not accurately reflect the regulation and/or interaction of the different isoforms with regulatory factors under native conditions in the intestine. One model that could be used to answer this question in mammals may be the *NHE3* gene-targeted mouse. This strain exhibits congenital diarrhea with severe intestinal absorptive deficits resulting from impaired transepithelial Na<sup>+</sup> movement (8) and given these results would seem to be a logical choice in which to examine dipeptide uptake and the pH<sub>i</sub> of intestinal enterocytes.

The advantages of working in a genomically defined and genetically amenable model organism have made possible the development of several novel systems for exploring ion trans-

port physiology. By using these systems, we hope to expand upon the role of Na<sup>+</sup>/H<sup>+</sup> exchangers in normal gut function, both in nematodes and, given the cross-species applicability of nematode research to date, mammals as well. Being able to measure the intracellular pH and changes in pH that occur during normal physiological processes should enhance our ability to pose questions regarding acid-base transport and its regulation in the intestine, as well as other cell types. In particular, in the future by using this technology we can place emphasis on studying ion transport processes that are coupled to behaviors that occur only in an intact organism.

*Acknowledgments*—I thank James Melvin for past and present support and Idalia Alaniz for technical assistance. Fred Hagen provided much of the necessary equipment for creation of the transgenic strains and their analysis, and Teresa Sherman displayed efforts well beyond the call of duty.

## REFERENCES

- Hayashi, H., Szaszi, K., and Grinstein, S. (2002) *Ann. N. Y. Acad. Sci.* **976**, 248–258
- Wakabayashi, S., Shigekawa, M., and Pouyssegur, J. (1997) *Physiol. Rev.* **77**, 51–74
- Orlowski, J., and Grinstein, S. (1997) *J. Biol. Chem.* **272**, 22373–22376
- Rossmann, H., Sonntag, T., Heinzmann, A., Seidler, B., Bachmann, O., Vieillard-Baron, D., Gregor, M., and Seidler, U. (2001) *Am. J. Physiol.* **281**, G447–G458
- Repishti, M., Hogan, D. L., Pratha, V., Davydova, L., Donowitz, M., Tse, C. M., and Isenberg, J. I. (2001) *Am. J. Physiol.* **281**, G159–G163
- Bachmann, O., Sonntag, T., Siegel, W. K., Lamprecht, G., Weichert, A., Gregor, M., and Seidler, U. (1998) *Am. J. Physiol.* **275**, G1085–G1093
- Muallem, S., Burnham, C., Blissard, D., Berglindh, T., and Sachs, G. (1985) *J. Biol. Chem.* **260**, 6641–6653
- Schultheis, P. J., Clarke, L. L., Meneton, P., Miller, M. L., Soleimani, M., Gawenis, L. R., Riddle, T. M., Duffy, J. J., Doetschman, T., Wang, T., Giebisch, G., Aronson, P. S., Lorenz, J. N., and Shull, G. E. (1998) *Nat. Genet.* **19**, 282–285
- Schultheis, P. J., Clarke, L. L., Meneton, P., Harline, M., Boivin, G. P., Stemmermann, G., Duffy, J. J., Doetschman, T., Miller, M. L., and Shull, G. E. (1998) *J. Clin. Invest.* **101**, 1243–1253
- Bell, S. M., Schreiner, C. M., Schultheis, P. J., Miller, M. L., Evans, R. L., Vorhees, C. V., Shull, G. E., and Scott, W. J. (1999) *Am. J. Physiol.* **276**, C788–C795
- Nehrke, K., and Melvin, J. E. (2002) *J. Biol. Chem.* **277**, 29036–29044
- Fei, Y. J., Kanai, Y., Nussberger, S., Ganapathy, V., Leibach, F. H., Romero, M. F., Singh, S. K., Boron, W. F., and Hediger, M. A. (1994) *Nature* **368**, 563–566
- Liang, R., Fei, Y. J., Prasad, P. D., Ramamoorthy, S., Han, H., Yang-Feng, T. L., Hediger, M. A., Ganapathy, V., and Leibach, F. H. (1995) *J. Biol. Chem.* **270**, 6456–6463
- Thwaites, D. T., Ford, D., Glanville, M., and Simmons, N. L. (1999) *J. Clin. Invest.* **104**, 629–635
- Anderson, C. M., Mendoza, M. E., Kennedy, D. J., Raldua, D., and Thwaites, D. T. (2003) *Br. J. Pharmacol.* **138**, 564–573
- Fei, Y. J., Romero, M. F., Krause, M., Liu, J. C., Huang, W., Ganapathy, V., and Leibach, F. H. (2000) *J. Biol. Chem.* **275**, 9563–9571
- Fei, Y. J., Fujita, T., Lapp, D. F., Ganapathy, V., and Leibach, F. H. (1998) *Biochem. J.* **332**, 565–572
- Miesenbock, G., De Angelis, D. A., and Rothman, J. E. (1998) *Nature* **394**, 192–195
- Granato, M., Schnabel, H., and Schnabel, R. (1994) *Nucleic Acids Res.* **22**, 1762–1763
- Mello, C. C., Kramer, J. M., Stinchcomb, D., and Ambros, V. (1991) *EMBO J.* **10**, 3959–3970
- Thomas, J. A., Buchsbaum, R. N., Zimmiak, A., and Racker, E. (1979) *Biochemistry* **18**, 2210–2218
- Kamath, R. S., Fraser, A. G., Dong, Y., Poulin, G., Durbin, R., Gotta, M., Kanapin, A., Le Bot, N., Moreno, S., Sohrmann, M., Welchman, D. P., Zipperlen, P., and Ahringer, J. (2003) *Nature* **421**, 231–237
- Fire, A., Xu, S., Montgomery, M. K., Kostas, S. A., Driver, S. E., and Mello, C. C. (1998) *Nature* **391**, 806–811
- Ashrafi, K., Chang, F. Y., Watts, J. L., Fraser, A. G., Kamath, R. S., Ahringer, J., and Ruvkun, G. (2003) *Nature* **421**, 268–272
- Houthoofd, K., Braeckman, B. P., Lenaerts, I., Brys, K., De Vreese, A., Van Eygen, S., and Vanfleteren, J. R. (2002) *Exp. Gerontol.* **37**, 1371–1378
- Larsen, P. L., and Clarke, C. F. (2002) *Science* **295**, 120–123
- Lakowski, B., and Hekimi, S. (1998) *Proc. Natl. Acad. Sci. U. S. A.* **95**, 13091–13096
- Klass, M. R. (1977) *Mech. Ageing Dev.* **6**, 413–429
- Avery, L. (1993) *Genetics* **133**, 897–917
- Sohal, R. S., and Weindruch, R. (1996) *Science* **273**, 59–63
- Tatar, M., Bartke, A., and Antebi, A. (2003) *Science* **299**, 1346–1351
- Sankaranarayanan, S., and Ryan, T. A. (2001) *Nat. Neurosci.* **4**, 129–136
- Machen, T. E., Leigh, M. J., Taylor, C., Kimura, T., Asano, S., and Moore, H. P. (2003) *Am. J. Physiol.* **26**, C205–C214
- Jankowski, A., Kim, J. H., Collins, R. F., Daneman, R., Walton, P., and Grinstein, S. (2001) *J. Biol. Chem.* **276**, 48748–48753
- Kerr, R., Lev-Ram, V., Baird, G., Vincent, P., Tsien, R. Y., and Schaefer, W. R.

- (2000) *Neuron* **26**, 583–594
36. Franks, C. J., Pemberton, D., Vinogradova, I., Cook, A., Walker, R. J., and Holden-Dye, L. (2002) *J. Neurophysiol.* **87**, 954–961
37. Samuel, A. D., Murthy, V. N., and Hengartner, M. O. (2001) *BMC Dev. Biol.* **1**, 8
38. Daniel, H., and Rubio-Aliaga, I. (2003) *Am. J. Physiol.* **284**, F885–F892
39. Boll, M., Markovich, D., Weber, W. M., Korte, H., Daniel, H., and Murer, H. (1994) *Pfluegers Arch.* **429**, 146–149
40. Thwaites, D. T., Kennedy, D. J., Raldua, D., Anderson, C. M., Mendoza, M. E., Bladen, C. L., and Simmons, N. L. (2002) *Gastroenterology* **122**, 1322–1333
41. Kennedy, D. J., Leibach, F. H., Ganapathy, V., and Thwaites, D. T. (2002) *Pfluegers Arch.* **445**, 139–146
42. Matyash, V., Geier, C., Henske, A., Mukherjee, S., Hirsh, D., Thiele, C., Grant, B., Maxfield, F. R., and Kurzchalia, T. V. (2001) *Mol. Biol. Cell* **12**, 1725–1736
43. Shim, Y. H., Chun, J. H., Lee, E. Y., and Paik, Y. K. (2002) *Mol. Reprod. Dev.* **61**, 358–366
44. Merris, M., Wadsworth, W. G., Khamrai, U., Bittman, R., Chitwood, D. J., and Lenard, J. (2003) *J. Lipid Res.* **44**, 172–181
45. Rogina, B., Reenan, R. A., Nilsen, S. P., and Helfand, S. L. (2000) *Science* **290**, 2137–2140
46. Knauf, F., Rogina, B., Jiang, Z., Aronson, P. S., and Helfand, S. L. (2002) *Proc. Natl. Acad. Sci. U. S. A.* **99**, 14315–14319
47. Fei, Y. J., Inoue, K., and Ganapathy, V. (2003) *J. Biol. Chem.* **278**, 6136–6144
48. Himukai, M., Suzuki, Y., and Hoshi, T. (1978) *Jpn. J. Physiol.* **28**, 499–510
49. Matthews, D. M., Addison, J. M., and Burston, D. (1974) *Clin. Sci. Mol. Med.* **46**, 693–705
50. Attaphitaya, S., Nehrke, K., and Melvin, J. E. (2001) *Am. J. Physiol.* **281**, C1146–C1157
51. Levine, S. A., Montrose, M. H., Tse, C. M., and Donowitz, M. (1993) *J. Biol. Chem.* **268**, 25527–25535
52. Orłowski, J. (1993) *J. Biol. Chem.* **268**, 16369–16377